Adsorption (2013) 19:225–233
DOI 10.1007/s10450-012-9444-9

In situ small angle X-ray scattering and benzene adsorption on polymer-based carbon hollow fiber membranes

Evangelos P. Favvas · Konstantinos L. Stefanopoulos · Sergios K. Papageorgiou · Athanasios C. Mitropoulos

Received: 26 September 2012 / Accepted: 8 November 2012 / Published online: 21 November 2012

Abstract The structural changes and the mechanism of benzene adsorption on microporous carbon hollow fiber membranes with different surface and pore network properties have been investigated by in situ small-angle X-ray scattering (SAXS) and benzene adsorption. Benzene adsorption measurements have been carried out in situ with SAXS alongside an adsorption/desorption isotherm cycle at 293 K with the aid of a specially constructed adsorption sample cell. In addition low-pressure C_6H_6 and high-pressure CO_2, CH_4 and N_2 adsorption isotherms have been performed. Two carbon hollow fiber membranes, both prepared by controlled pyrolysis procedures of polyimide membrane precursor, were under study. During benzene adsorption the intensity of the SAXS curves changes in a way that depends on how the pores are filled and the contrast fluctuations occur. The SAXS data have been modeled by evaluating the form factor of lamellar micropores upon filling with C_6H_6. The existence of ultra micropores within the surrounding matrix was also taken into account. The results suggest that the arrangement of the ultra micropores on the non-activated membrane is in such a way that the access of benzene to the micropores is restricted, resulting in an incomplete filling. On the other hand, the activation process generates a more accessible pore network where the micropores are completely filled.

Keywords In situ · SAXS · Carbon membranes · Adsorption · Lamellar pore · Form factor

1 Introduction

Porous materials have received a great deal of attention due to their many applications (Ishizaki et al. 1998). These applications cover a wide range of both laboratory and industrial processes. The food industry, the biomedicine, the pharmaceutics technology as well the road maintenance, the ceramic products, the wood processing, the building materials and additionally the chemical separation and distillation processes, the mineralogy, the catalysts, the exploring materials, the natural gas and oil production are only some examples of porous materials applications. Further, porous carbon materials are appropriate for a major part of the aforementioned applications because of their low cost and their well-defined properties both in the case of sorbents and membranes (Hatori et al. 2004). One of the most important characteristics of carbons and activated carbons is the ability to adsorb optionally gas or vapors. Carbon membranes are more resistant when exposed to organic vapors or solvents, are not oxidized by acids or alkalis, they adsorb well various gases and they are highly hydrophobic. Moreover, the pore size in carbon membranes can be "finely adjusted" by selecting the nature of the precursor and by varying its pyrolysis parameters, as well as through the use of special techniques leading to a uniform pore size distribution. To this end activation processes such as CO_2, KOH, H_2O etc. environments can change the porous network or the average size of carbon materials by improving their properties

E.P. Favvas (✉) · K.L. Stefanopoulos · S.K. Papageorgiou
Institute of Physical Chemistry, NCSR Demokritos, Ag. Paraskevi Attikis, 153 41, Athens, Greece
e-mail: favvas@chem.demokritos.gr

K.L. Stefanopoulos (✉)
e-mail: stefan@chem.demokritos.gr

A.C. Mitropoulos
Department of Petroleum & Natural Gas Technology, Cavala Institute of Technology, Ag. Loukas, 65404, Cavala, Greece

(permeability, adsorption capacity etc.). On the other hand, microporous carbon membranes can be used for gas separation processes such as hydrogen production, oxygen production, carbon dioxide removal etc. (Favvas et al. 2007). These properties range the carbon membranes as one of the more popular materials for membrane research community.

An advanced and detailed characterization of structure and properties is a major challenge of optimization of materials preparation process. Small-angle scattering of neutrons or X-rays (SANS or SAXS) (Ramsay 1998; Mitropoulos et al. 1998a; Makri et al. 2000; Hoinkis et al. 2004), contrast-matching SANS (Steriotis et al. 2002a; Calo and Hall 2004; Mergia et al. 2010; Stefanopoulos et al. 2011) and adsorption in conjunction with neutron (X-ray) diffraction or SANS (SAXS) (Mitropoulos et al. 1998b; Steriotis et al. 2002b, 2004; Muroyama et al. 2008; Jähnert et al. 2009) have been proved to be essential tools for elucidating the microstructure of nanoporous materials, the adsorption mechanism and the properties of confined phases within the pores. The enhanced information obtained by such combined methods has motivated the development of several adsorption in situ scattering set-ups and cells (Katsaros et al. 2000; Hofmann et al. 2005).

In previous works, László et al. reported characterization of polymer-based (László et al. 2005, 2008; László and Geissler 2006) and high surface area commercial carbon materials (László et al. 2010) using water adsorption and SAXS. In specific, the SAXS measurements have been carried out by using sealed samples previously equilibrated at various relative pressures. In the present study, in situ measurements of benzene adsorption and SAXS have been performed on two polymer-based carbon hollow fiber membranes; one was prepared in inert Ar environment up to 1323 K and the other was an activated carbon hollow fiber membrane. For the performance of the in situ SAXS experiment, a specially designed sample cell has been constructed. Similar to other works, benzene was the adsorbate of choice because of its good affinity in carbon's walls (Dubinin 1960). In the following, the benzene adsorption isotherms and the experimental SAXS curves from both samples during the adsorption-desorption cycle will be presented and discussed together with the development of a realistic scattering model for evaluation of the form factor of lamellar pores upon benzene filling.

2 Experimental

BTDA-TDI/MDI (P84), co-polyimide hollow fibers were developed by the dry/*wet* phase inversion process via spinodal decomposition mechanism (Favvas et al. 2007). The involved spinning set up is already described in a previous work (Favvas et al. 2008). The as produced polymeric co-polyimide precursors were further pyrolized, under controlled conditions, to develop the asymmetric carbon membranes. In all cases, a pre-weighed batch of co-polyimide hollow fibers (P1) was placed in the quartz tube of a Carbolite CTF 12/75 High Temperature Furnace, equipped with a Eurotherm 2408CP temperature controller. Membrane 1 (M1) was pyrolyzed at a heating rate of 5 K/min up to 1323 K with 150 ml/min of Ar sweeping the inner side of the furnace tube, stabilization at the maximum temperature for 4 h and cooling down to 298 K with a rate of 5 K/min. The total weigh loss is 45.42 % whereof 3 % occur during the isothermal stay of 1323 K. The pyrolytic procedure followed for the activated membrane (M2) was similar to this for M1. The subsequent activation process was carried out after completion of the isothermal pyrolysis step, by switching to 150 ml/min of CO_2 for one min. An extra weight loss of 1 % occurs in membrane M2 derive from the effect of CO_2 stream after the isothermal process. Thus, the total weight loss of M2 membrane, during carbonization process, was 46.42 % and the 1 % referred in the action of the CO_2 stream for only 1 minute at the highest temperature.

The low-pressure benzene adsorption/desorption isotherm, on vapor phase, was obtained using a homemade stainless steel gravimetric rig at 293 K. The balance head (CI Microbalances), counterweight compartment, valves and tubing of the system were thermostated in an air-circulating bath ($\pm$0.1 K), whereas the sample compartment was separately thermostated in a silicon oil bath ($\pm$0.01 K). The high-pressure (0.01–10 MPa) adsorption CO_2, CH_4 and N_2 isotherms at 273 and 298 K were measured via a magnetic suspension balance (Rubotherm). Buoyancy corrections have been taken into account.

The X-ray diffraction (XRD) patterns were recorded on a Siemens XD-500 diffractometer using CuKα X-ray source. The in situ adsorption/SAXS measurements were carried out at 293 K using a Rigaku system (SMAX-300) provided by JJ X-Ray Systems, connected to a sealed tube CuKα X-ray generator. The specially designed sample cell comprises of two separate parts that are secured with M6 bolts, to ensure a tight sealing of the two parts—this enables the application of pressure to a rubber O-ring that maintains the necessary vacuum ($\sim 10^{-4}$ Torr) for adsorption experiments. The bottom part of the specimen cell has an embedded pipe that runs around the specimen holder chamber and is thermostated using a heater–freezer Julabo circulator. The cell windows are covered with Mylar sheets. Silver behenate has been used as a standard SAXS calibrant for evaluating the scattering vector, Q from the sample-to-detector distance ($Q = 4\pi \sin\theta/\lambda$, where λ and 2θ are the wavelength and the scattering angle respectively). The Q range varied approximately between 0.02 to 0.5 Å^{-1}. Before putting the samples into the cell, they were granulated using a porcelain Petri until the grain size appointed to the average size

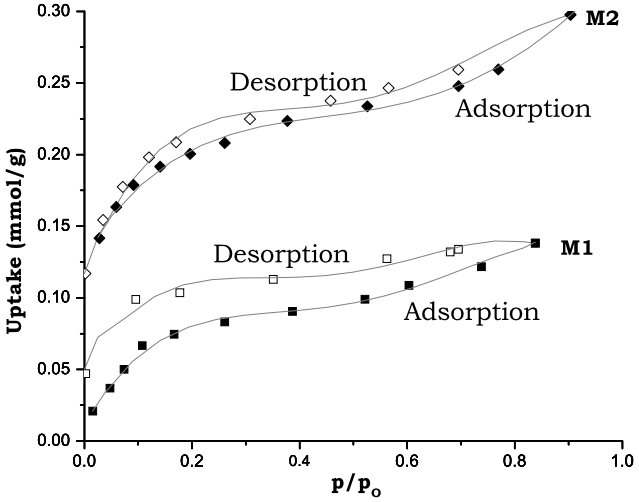

Fig. 1 Benzene adsorption isotherms at 293 K for the samples *M1* and *M2*. *Lines* have been used as a guide to the eye

of about 140 mesh. Afterwards they were evacuated in a glass cell up to 250 °C under high vacuum conditions (up to 10^{-7} mbar) using a turbo vacuum pump for 24 h. During the in situ adsorption with SAXS experiments the samples were equilibrated, at least, for 24 h for each equilibrium pressure. Finally the raw data were corrected for instrumental background and scattering of the empty cell.

3 Results and discussion

3.1 Adsorption isotherms

Figure 1 illustrates the benzene adsorption isotherms at 293 K for the M1 and M2 samples. Both isotherms are closer to type IIb according to the IUPAC classification (Sing et al. 1985). The very low total adsorbed amounts, in both cases, combined with observable hysteresis loops imply that the pore network consists mainly from ultra micropores (Setoyama et al. 1996; Benadjemia et al. 2011).

Figure 1 clearly shows a significant remaining adsorbed amount of benzene, after the completion of desorption process, corresponding to about one third of the total uptake for both M1 and M2 samples. This result can be explained in terms of the carbon microstructure (especially in the areas where constrictions and ink-like pores are present) that blocks the adsorbate molecules to remove out of the sample. This phenomenon persists even if the sample is under vacuum for 48 h or even by increasing the temperature up to 373 K. The remaining amount of benzene after an adsorption/desorption cycle will also be verified by the in situ SAXS measurements. Finally, the total uptake in the case of M2 sample is significantly higher, due to a more accessible pore volume created possibly by the activation process

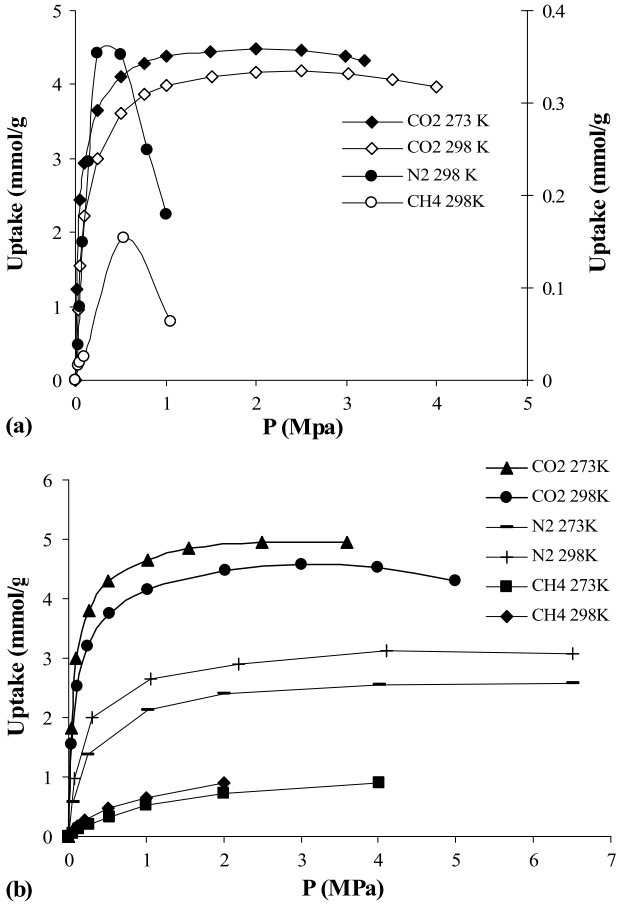

Fig. 2 High-pressure adsorption isotherms (**a**) M1 membrane CO_2 (273 and 298 K), CH_4 and N_2 (298 K) and (**b**) M2 membrane CO_2, CH_4 and N_2 (273 and 298 K). Note that in Fig. 2a the *dotted lines* are referred to *y*-axis on the right side of the plot

(Pérez-Mendoza et al. 2006). Indeed, the calculation of the pore volumes derived from the isotherms ($p/p_0 = 0.8$) are about 0.01 and 0.02 cm^3/g respectively for the M1 and M2 membranes. In addition, the initial steep rise of the isotherm in the case of the activated sample is slightly moved towards higher relative pressures suggesting an increase of the micropore size.

Adsorption experiments of N_2 at 77 K were initially conducted in order to define the BET surface area and the microporosity of the carbon hollow fiber membranes. However, the pertinent measurement has revealed negligible uptake of N_2 at 77 K. The existence of ultra micropores has also been confirmed by excess adsorption isotherms (GSE) of CO_2, CH_4 and N_2 up to 10 MPa on both carbon membranes. The surface excess adsorption of CO_2 on fiber M1 (Fig. 2a), increases at the low-pressure region, reaches a plateau and then slightly decreases with increasing pressure. The shape of the adsorption curve is expected, according to the definition of the surface excess for a pure gas (Sircar 1999). A similar shape was observed for N_2 and CH_4 on M1 at 298 K (Fig. 2a), although in this case, the adsorption max-

imum occurred at very low pressures and the decrease at higher pressures was much more pronounced, resulting in almost zero values of mass uptake. It should be also noted that in case of N_2 and CH_4 at 273 K the total adsorbate mass was zero even if the pressure increased up to 10 MPa. This indicates that the structural arrangement of the ultra micropores in M1 membrane inhibits the diffusion of CH_4 and N_2 molecules at 273 K. In the case of M2, however, the absence of phenomena such as the almost zero mass uptake suggests that the ultra micropore size must be larger than that of the precursor fiber M1 (Fig. 2b). Another important observation is that the N_2 and CH_4 adsorption isotherms did not follow the usual exothermic character of adsorption. In this case the increase of temperature had a beneficial effect on the adsorbed quantity. The term "activated sorption" is given to this type of adsorption, which is characteristic of the existence of a large number of constrictions and diffusion obstructions in the porous matrix.

In a previous work, H_2 adsorption-desorption measurements (77 K) were carried out (Favvas et al. 2008). The small size of H_2 molecules and the fact that the temperature is by far above their supercritical temperature ensures that even the smallest pores, possibly not accessible to other molecules, would easily be monitored, while equilibration kinetics are expected to be fast enough for reliable measurements. The results suggested that the pore network of the M1 is highly super-microporous and the adsorption desorption isotherm of H_2 at 77 K presented a large hysteresis loop. On the other hand, in case of M2 membrane the loop occurred extremely narrow because of the larger and more accessible pore network due to activation process.

3.2 In situ SAXS and benzene adsorption

Figure 3 shows the SAXS curves of the dry M1 and M2 samples. The shape of the scattering curves is typical for polymer-based carbons (László et al. 2005, 2008; László and Geissler 2006). In the low-Q region the spectra are dominated by surface scattering from the interfaces between the micron-sized sub-grains, as revealed by scanning electron microscopy (SEM) studies (Favvas et al. 2011). In the case of M1 membrane the power-law behavior, $I(Q) \propto Q^{-4}$ (Porod's law), is attributed to scattering from smooth interfaces (Porod 1982). However, when the surface texture is rough the value of the exponent varies between 3 and 4 (Bale and Schmidt 1984), as observed for the M2 sample ($I(Q) \propto Q^{-3}$). A possible explanation for the surface roughness, also observed by SEM (Favvas et al. 2011), could be the enhanced microporosity of the outer skin layer induced by the CO_2 activation process. The plateau in the intermediate Q-region followed by the shoulder is characteristic for the microporous structure of the samples. From the curvature of the shoulder in the SAXS curves one may

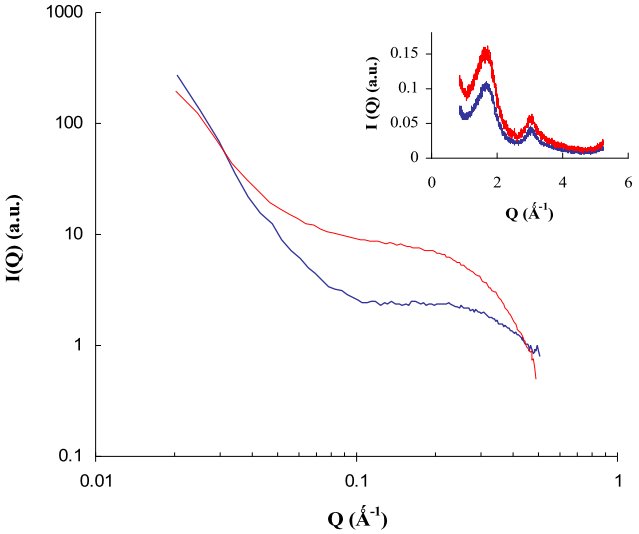

Fig. 3 Benzene SAXS patterns and (*inset*) XRD spectra of dry M1 (*lower curves*) and M2 (*upper curves*) samples

calculate the Guinier radius of gyration (R_G) (Porod 1982). The resulting values of R_G are 4.1 and 5.7 Å for M1 and M2 respectively. This is reasonable as one expects an increase of the mean pore size in the case of the activated sample. However, the extracted values are significant only for comparison reasons but they are not reliable because the Guinier expression is not valid for dense and polydisperse systems.

In the inset of Fig. 3, the high-Q region of the carbon membranes was obtained by XRD patterns. The broad peaks observed are residues of the main diffraction peaks of graphite. In addition, the similarity of the Bragg peaks suggests that the activation with CO_2 (M2) had no effect on the structure of the developed material. The first reflection, corresponding to a d-spacing of 3.72 Å, is evidential of the turbostratic structure (random layer lattice) (Zhang et al. 2006; Dahn et al. 1997) while the second one coincides with the third characteristic X-ray diffraction peak for the pure pyrolytic graphite powder (Jianqing 1993) with a d-spacing of 2.06 Å. Introduction of heteroatoms into the turbostratic layers renders the carbon surface more attractive to polar molecules. The most common heteroatom in the carbon matrix is oxygen, which generally bonds along the edges of the graphene layers.

The in situ SAXS measurements of M1 membrane during a complete benzene adsorption-desorption cycle are illustrated in Fig. 4. The SAXS patterns show interesting features during the filling process. More specific, the curves of the *wet* sample, upon adsorption (Fig. 4a), during all pressure steps, exceed that of the dry one in the range $0.06 < Q < 0.39$ Å^{-1}. The larger increase in intensity occurs during the first adsorption step ($p/p_0 = 0.14$). On the other hand, for the high-Q region ($Q > 0.39$ Å^{-1}) the scattered intensity of the *wet* sample lies below that of the dry and remains practically unaltered for all the relative pressures.

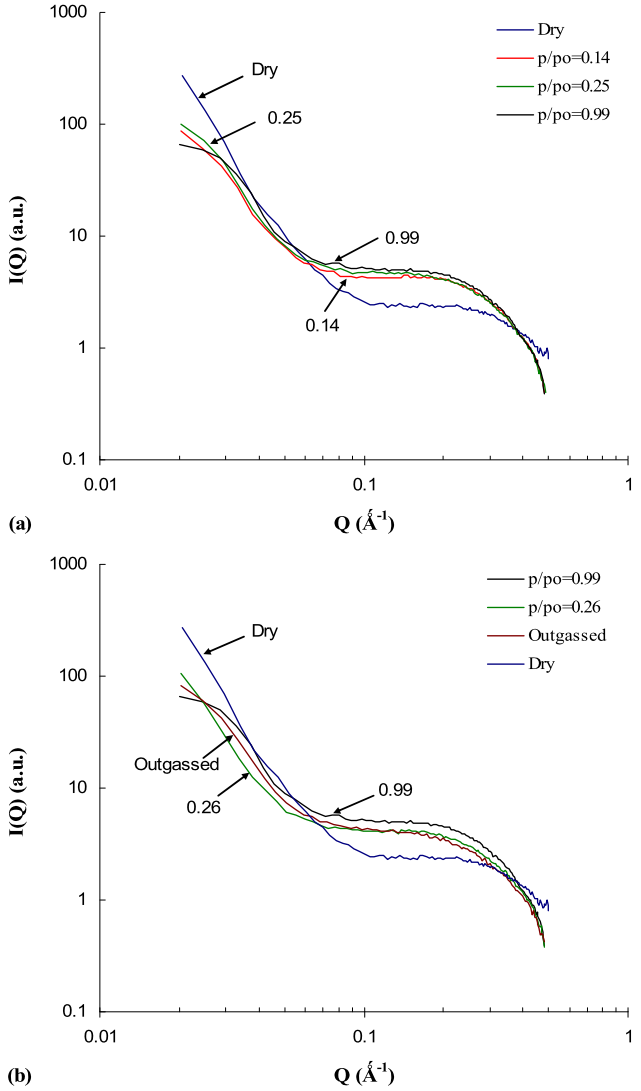

Fig. 4 In situ SAXS curves of M1 sample during an (**a**) adsorption and (**b**) desorption cycle

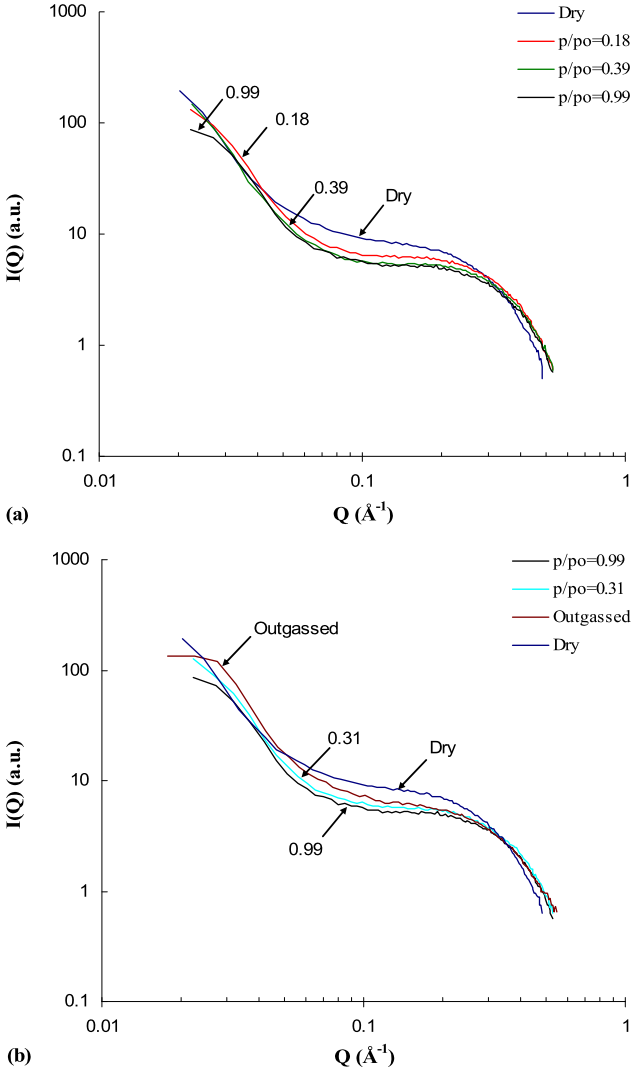

Fig. 5 In situ SAXS curves of M2 sample during an (**a**) adsorption and (**b**) desorption cycle

One may then claim that the filling mechanism has almost fulfilled at $p/p_0 = 0.14$. The result is in agreement with the adsorption isotherm where the steep increase is observed up to about $p/p_0 = 0.11$.

During the desorption process ($p/p_0 = 0.26$), a small decrease in intensity is observed ($0.06 < Q < 0.39$ Å^{-1}) compared to the fully *wet* sample ($p/p_0 = 0.99$); in addition the SAXS signal does not change at the high-Q region. Further, the scattering curve from the outgassed sample ($p/p_0 = 0$) does not differ significantly to that at $p/p_0 = 0.26$, suggesting that a benzene amount still remains. This result is also in excellent agreement with the adsorption isotherm. The scattering curve of the dry sample is also presented in Fig. 4b for comparison reasons.

Figure 5 shows the in situ SAXS spectra of M2 sample. In this case, the SAXS curves, upon adsorption (Fig. 5a), lie below that of the dry sample in the region $0.04 < Q <$ 0.27 Å^{-1}. Further, at $Q > 0.27$ Å^{-1}, the intensity of *wet* sample exceeds that of the dry at all relative pressures and remains almost unchanged. In a similar way to M1 membrane, the SAXS patterns show that the filling process has almost been completed during the second adsorption step ($p/p_0 = 0.39$), in agreement with the benzene isotherm. As desorption progresses a small increase of the scattered intensity ($0.04 < Q < 0.27$ Å^{-1}) is observed while the intensity in the high-Q region remains unaltered (Fig. 5b). Again, the SAXS pattern from the outgassed sample differs significantly compared to that of the dry sample confirming the isotherm result for a remaining C_6H_6 amount.

3.3 SAXS model for lamellar pores

László and co-workers (László et al. 2005, 2008; László and Geissler 2006) interpreted their SAXS results of water vapor adsorption in microporous carbons in terms of a non-

uniform pore filling. The derived density function, $p(Q)$, is a direct measure in reciprocal space of the relative mass (or electronic) density of the fluid with respect to the bulk liquid; in principle, $0 \leq p(Q) < 1$ when the pores are incompletely filled and $p(Q) = 1$ for complete pore filling. The shape of the density functions can thus provide information about the filling process. However, in the regions where the scattered intensity of the *wet* samples exceeds that of the dry system, $p(Q)$ takes negative values and the model is not valid.

In the present study, we attempt to model the SAXS data by assuming a more realistic approach based on adsorption of lamellar (slit-like) pores. According to the small-angle theory (of X-rays or neutrons respectively), the scattered intensity, $I(Q)$, of randomly oriented lamellar scatterers can be written as (Nallet et al. 1993):

$$I(Q) = \frac{\pi}{WQ^2} P(Q) S(Q) \tag{1}$$

where $2W$ is the pore width, $P(Q)$ is the pore form factor and $S(Q)$ is the structure factor arising from interference effects in the scattering from pores which are in close separation.

The form factor of randomly oriented lamellar pores filled with two different adsorbates was derived in a way similar to the form factor of isotropically averaged bilayers (Nallet et al. 1993; Skouri et al. 1991):

$$P(Q) = \frac{4}{Q^2}\Big\{(\rho_1 - \rho_2)\sin(QW) + (\rho_3 - \rho_1)\sin\big[Q(W-t)\big]\Big\}^2 \tag{2}$$

where t is the thickness of the adsorbed phase at the outer layer of the pore with electron density (or scattering length density in the case of neutrons) ρ_1, ρ_3 is the electron density of the adsorbed phases at the inner layer of the pore and ρ_2 is the electron density of the surrounding solid matrix (Fig. 6a). Note that in case of micropores, t, is referred to the thickness of the adsorbed layer.

In our case, benzene is the only adsorbate of choice; thus, following Eq. (2) the filling process can be described as:

$$P(Q) = \frac{4}{Q^2}\Big\{(\rho_b - \rho_{cm})\sin(QW) - \rho_b \sin\big[Q(W-t)\big]\Big\}^2 \tag{3}$$

where $\rho_1 = \rho_b$, $\rho_2 = \rho_{cm}$ and $\rho_3 = \rho_p = 0$ are the electron densities of the benzene, the carbon matrix and the empty pore respectively (Fig. 6b). Thus, the filling process can be expressed by the ratio of form factors:

$$\frac{P(Q)_{wet}}{P(Q)_{dry}} = \left\{\frac{(\rho_b - \rho_{cm})\sin(QW) - \rho_b \sin[Q(W-t)]}{-\rho_{cm}\sin(QW)}\right\}^2 \tag{4}$$

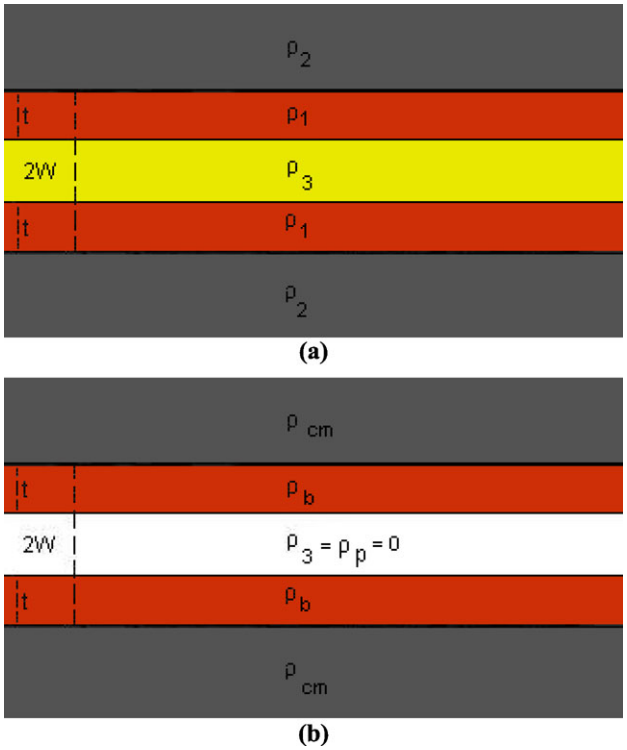

Fig. 6 Schematic profile of a lamellar pore structure (**a**) filled with two adsorbates and (**b**) partial filled with benzene; see text for details

A Gaussian distribution of the pore width and the thickness of the adsorbed phase can be further used for taking polydispersity into account (half-width at half maximum σ_{2W} and σ_t respectively) (Salvati et al. 2007). By assuming that the carbon structure is not altered by the adsorbed molecules (László et al. 2005, 2008; László and Geissler 2006), the form factor ratio can be approximated by the intensity ratio.

In a previous study (Zickler et al. 2006), SAXS experiments of C_5F_{12} adsorption on ordered mesoporous silica SBA-15 have been performed. The pore filling mechanism was described by calculating the form factor of cylindrical shells with various electron densities including the assumption of a lower-density layer, namely corona (Impéror-Clerc et al. 2000). In another work, SAXS results of nitrogen adsorption on ordered mesoporous silica MCM-41 were also analyzed by taking into account the existence micropores surrounding the cylindrical mesopores (Albouy and Ayral 2002). In a similar way, we are now considering that the carbon matrix is consisted of ultra micropores having porosity ε; the electron density of the carbon matrix before adsorption can be written as:

$$\rho_{cm} = (1 - \varepsilon)\rho_c \tag{5}$$

where ρ_c is the electron density of carbon; during adsorption, it can be expressed as:

$$\rho_{cm} = (1 - \varepsilon)\rho_c + \varepsilon\rho_b \quad (6)$$

The application of the proposed model (Eqs. (4)–(6)) justifies the intensity increase in some regions of the scattering curve of the *wet* samples. Besides the case of polymer-based microporous carbons (see also László et al. 2008), in situ SANS measurements and nitrogen physisorption in hierarchical porous silica also revealed an intensity increase at low relative pressures (Sel et al. 2007). The source of this extra scattering was attributed to the filling of micropores and small mesopores. In another study, in situ neutron diffraction measurements of carbon dioxide adsorption on MCM-41 have been carried out; an increase of the (10) Bragg peak intensity was observed during the first adsorption stage (5 bar) (Steriotis et al. 2008). The interpretation of the results favored the development of an adsorbed monolayer without excluding the existence of a corona surrounding the pores.

Our experimental data were fitted for both samples during the last adsorption stage ($p/p_0 = 0.99$), according to the proposed model. The model has been applied only for the saturated case because, as previously discussed, both the adsorption isotherms and the scattering curves suggest that the filling process has been almost completed during the initial adsorption stages. The electron densities used for our calculations were $\rho_b = 2.84 \times 10^{23}$ cm^{-3} and $\rho_c = 6.32 \times 10^{23}$ cm^{-3} for benzene and carbon respectively. In the case of M1 membrane the best fit was obtained by considering an array of polydisperse distribution of lamellar micropores ($2W = 18$ Å, $\sigma_{2W} = 11$ Å) partially filled with C_6H_6 molecules having thickness $t = 4.8$ Å ($\sigma_t = 0.3$ Å) (Fig. 7a). Since the critical size of benzene molecule is 5.9 Å, one may assume that formation of a monolayer on the pore walls takes place. This effect has also been observed in graphite slit micropores studied with GCMC simulations (Ohba et al. 2000). One may also note that we are dealing with micropores belonging to the micropore/mesopore region according to the IUPAC classification (Sing et al. 1985). From this point of view the existence of an adsorbed layer cannot be excluded. The surrounding carbon matrix is consisted of ultra micropores ($\varepsilon = 0.55$) filled with benzene. The monolayer coverage of the micropores could be attributed to the constrictions probably caused by the presence of the ultra micropores as illustrated in the inset of Fig. 7a.

In the case of M2 sample, however, the activation process generates a more accessible network (Pérez-Mendoza et al. 2006) resulting in the complete filling of the micropores (Fig. 7b). A small tendency for increasing size, $2W$, and porosity, ε, could also be attributed to CO_2 activation; $2W = 20.5$ Å ($\sigma_{2W} = 6$ Å), $t = 10.25$ Å ($\sigma_t = 3$ Å), $\varepsilon = 0.58$. In addition, the small difference in porosities can

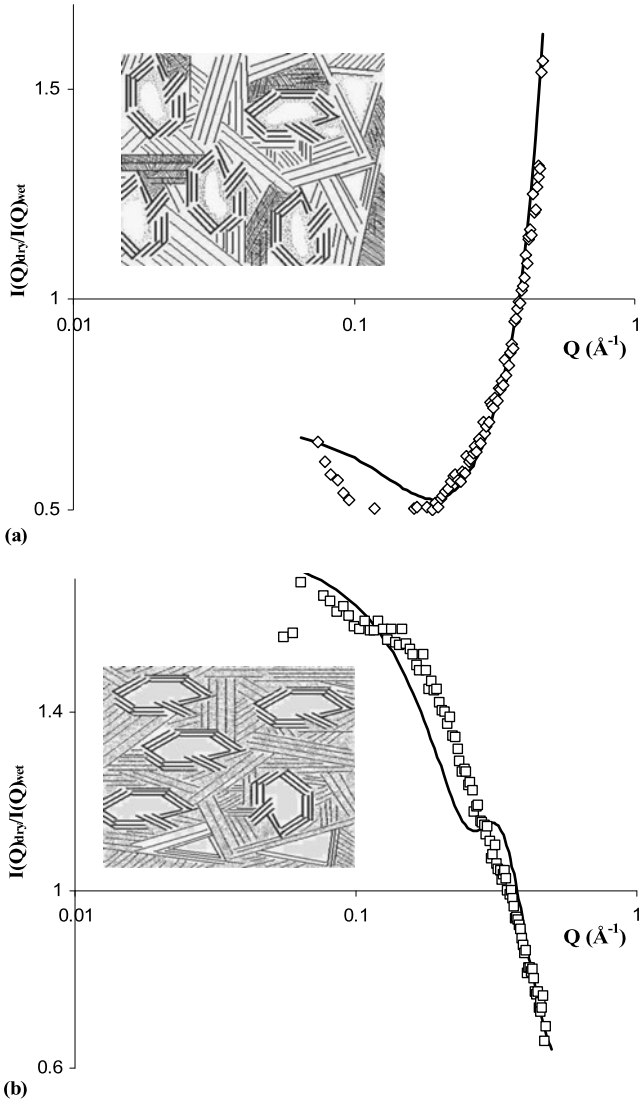

Fig. 7 Experimental SAXS curves (*points*) and fitted curves (*lines*) for (**a**) M1 and (**b**) M2 samples and (*insets*) their proposed structural representation; see text for details

be explained in terms of the low burn off (1 %) on M2 carbon fiber because only few surface end-chains and constrictions were removed during the activation process. Finally in both membranes (especially M2), some deviations of the fitted curves from the experimental data are observed. A possible explanation could be the non-uniform distribution of the ultra micropores within the carbon matrix. Further, the activation process seems to enhance this effect in the case of M2 membrane.

4 Conclusions

In the present study in situ SAXS measurements have been carried out during a complete benzene adsorption-desorption cycle for two different polymer-based carbon

hollow fiber membranes. These membranes are good candidates for high efficiency industrial processes, such as hydrogenation and natural gas enrichment. The experiment performed with the aid of a specially designed sample cell. In addition, the samples have been characterized by gas adsorption isotherms and XRD measurements. Both SAXS patterns and benzene adsorption isotherms suggest that the filling mechanism is almost completed at low relative pressures. Moreover, upon completion of the desorption process, a remaining benzene amount is observed. The SAXS measurements have also displayed differences in the way benzene is adsorbed by the two samples. The SAXS patterns have been modeled by evaluating the form factor of a lamellar micropore upon C_6H_6 filling. In addition, the existence of ultra micropores within the surrounding matrix was taken into account. In the case of the non-activated carbon membrane a partial filling of the micropores (monolayer coverage) is concluded due to constrictions probably caused by the presence of the ultra micropores. On the other hand, the activation process generates a more accessible network resulting in the complete filling of the micropores. The proposed model could be expanded to lamellar structures such as lamellar polymers, block copolymers, composites and clays.

Acknowledgements The authors would like to thank Dr. T.A. Steriotis for useful discussions. E.P. Favvas, K.L. Stefanopoulos and A.C. Mitropoulos would also like to acknowledge Thalis "NANOCAPILLARY MIS 375233" and Archimedes "NANO-SKAI" research projects of the Greek Ministry of National Education and Religious Affairs for the funding of the present study.

References

Albouy, P.-A., Ayral, A.: Coupling X-ray scattering and nitrogen adsorption: an interesting approach for the characterization of ordered mesoporous materials. Application to hexagonal silica. Chem. Mater. **14**, 3391–3397 (2002)

Bale, H.D., Schmidt, P.W.: Small-angle X-ray-scattering investigation of submicroscopic porosity with fractal properties. Phys. Rev. Lett. **53**, 596–599 (1984)

Benadjemia, M., Millière, L., Reinert, L., Benderdouche, N., Duclaux, L.: Preparation, characterization and methylene blue adsorption of phosphoric acid activated carbons from globe artichoke leaves. Fuel Process. Technol. **92**, 1203–1212 (2011)

Calo, J.M., Hall, P.J.: The application of small angle scattering techniques to porosity characterization in carbons. Carbon **42**, 1299–1304 (2004)

Dahn, J.R., Xing, W., Gao, Y.: The "falling cards model" for the structure of microporous carbons. Carbon **35**, 825–830 (1997)

Dubinin, M.M.: The potential theory of adsorption of gases and vapors for adsorbents with energetically nonuniform surfaces. Chem. Rev. **60**, 235–241 (1960)

Favvas, E.P., Kapantaidakis, G.C., Nolan, J.W., Mitropoulos, A.C., Kanellopoulos, N.K.: Preparation, characterization and gas permeation properties of carbon hollow fiber membranes based on Matrimid® 5218 precursor. J. Mater. Process. Technol. **186**, 102–110 (2007)

Favvas, E.P., Kouvelos, E.P., Romanos, G.E., Pilatos, G.I., Mitropoulos, A.C., Kanellopoulos, N.K.: Characterization of highly selective microporous carbon hollow fiber membranes prepared from a commercial co-polyimide precursor. J. Porous Mater. **15**, 625–633 (2008)

Favvas, E.P., Romanos, G.E., Papageorgiou, S.K., Katsaros, F.K., Mitropoulos, A.C., Kanellopoulos, N.K.: A methodology for the morphological and physicochemical characterisation of asymmetric carbon hollow fiber membranes. J. Membr. Sci. **375**, 113–123 (2011)

Hatori, H., Takagi, H., Yamada, Y.: Gas separation properties of molecular sieving carbon membranes with nanopore channels. Carbon **42**, 1169–1173 (2004)

Hofmann, T., Wallacher, D., Huber, P., Birringer, R., Knorr, K., Schreiber, A., Findenegg, G.H.: Small-angle X-ray diffraction of Kr in mesoporous silica: effects of microporosity and surface roughness. Phys. Rev. B **72**, 064122 (2005)

Hoinkis, E., Lima, E.B.F., Schubert-Bischoff, P.: A study of carbon black Corax N330 with small-angle scattering of neutrons and X-rays. Langmuir **20**, 8823–8830 (2004)

Impéror-Clerc, M., Davidson, P., Davidson, A.: Existence of a microporous corona around the mesopores of silica-based SBA-15 materials templated by triblock copolymers. J. Am. Chem. Soc. **122**, 11925–11933 (2000)

Ishizaki, K., Komarneni, S., Nanko, M.: Porous Materials: Process, Technology and Applications. Kluwer Academic, Netherlands (1998)

Jähnert, S., Müter, D., Prass, J., Zickler, G.A., Paris, O., Findenegg, G.H.: Pore structure and fluid sorption in ordered mesoporous silica. I. Experimental study by in situ small-angle X-ray scattering. J. Phys. Chem. C **113**, 15201–15210 (2009)

Jianqing, J.: On the crystal orientation of graphite lamellae in unidirectionally solidified Fe-C eutectic alloy. J. Mater. Sci. Lett. **12**, 1861–1863 (1993)

Katsaros, F.K., Steriotis, T.A., Stefanopoulos, K.L., Kanellopoulos, N.K., Mitropoulos, A.C., Meissner, M., Hoser, A.: Neutron diffraction study of adsorbed CO_2 on a carbon membrane. Physica B **276–278**, 901–902 (2000)

László, K., Geissler, E.: Surface chemistry and contrast-modified SAXS in polymer-based activated carbons. Carbon **44**, 2437–2444 (2006)

László, K., Czakkel, O., Josepovits, K., Rochas, C., Geissler, E.: Influence of surface chemistry on the SAXS response of polymer-based activated carbons. Langmuir **21**, 8443–8451 (2005)

László, K., Rochas, C., Geissler, E.: Water vapour adsorption and contrast-modified SAXS in microporous polymer-based carbons of different surface chemistry. Adsorption **14**, 447–455 (2008)

László, K., Czakkel, O., Dobos, G., Lodewyckx, P., Rochas, C., Geissler, E.: Water vapour adsorption in highly porous carbons as seen by small and wide angle X-ray scattering. Carbon **48**, 1038–1048 (2010)

Makri, P.K., Stefanopoulos, K.L., Mitropoulos, A.C., Kanellopoulos, N.K., Treimer, W.: Study on the entrapment of mercury in porous glasses by neutron scattering in conjunction with mercury porosimetry. Physica B **276–278**, 479–480 (2000)

Mergia, K., Stefanopoulos, K.L., Ordás, N., García-Rosales, C.: A comparative study of the porosity of doped graphites by small angle neutron scattering, nitrogen adsorption and helium pycnometry. Microporous Mesoporous Mater. **134**, 141–149 (2010)

Mitropoulos, A.C., Kanellopoulos, N.K., Stefanopoulos, K.L., Heenan, R.K.: Scattering by curved and fractal surfaces. J. Colloid Interface Sci. **203**, 229–230 (1998a)

Mitropoulos, A.C., Stefanopoulos, K.L., Kanellopoulos, N.K.: Coal studies by small angle X-ray scattering. Microporous Mesoporous Mater. **24**, 29–39 (1998b)

Muroyama, N., Yoshimura, A., Kubota, Y., Miyasaka, K., Ohsuna, T., Ryoo, R., Ravikovitch, P.I., Neimark, A.V., Takata, M.,

Terasaki, O.: Argon adsorption on MCM-41 mesoporous crystal studied by in situ synchrotron powder X-ray diffraction. J. Phys. Chem. C **112**, 10803–10813 (2008)

Nallet, F., Laversanne, R., Roux, D.: Modelling X-ray or neutron scattering spectra of lyotropic lamellar phases: interplay between form and structure factors. J. Phys., II **3**, 487–502 (1993)

Ohba, T., Suzuki, T., Kaneko, K.: Preformed monolayer-induced filling of molecules in micropores. Chem. Phys. Lett. **326**, 158–162 (2000)

Pérez-Mendoza, M., Schumacher, C., Suárez-García, F., Almazán-Almazán, M.C., Domingo-García, M., López-Garzón, F.J., Seaton, N.A.: Analysis of the microporous texture of a glassy carbon by adsorption measurements and Monte Carlo simulation. Evolution with chemical and physical activation. Carbon **44**, 638–645 (2006)

Porod, G.: General Theory. In: Glatter, O., Kratky, O. (eds.) Small Angle X-Ray Scattering, pp. 17–51. Academic Press, London (1982)

Ramsay, J.D.F.: Surface and pore structure characterisation by neutron scattering techniques. Adv. Colloid Interface Sci. **76–77**, 13–37 (1998)

Salvati, A., Ristori, S., Oberdisse, J., Spalla, O., Ricciardi, G.: Small angle scattering and zeta potential of liposomes loaded with octa(carboranyl)porphyrazine. J. Phys. Chem. B **111**, 10357–10364 (2007)

Sel, O., Brandt, A., Wallacher, D., Thommes, M., Smarsly, B.: Pore hierarchy in mesoporous silicas evidenced by in-situ SANS during nitrogen physisorption. Langmuir **23**, 4724–4727 (2007)

Setoyama, N., Kaneko, K., Rodriguez-Reinoso, F.: Ultramicropore characterization of microporous carbons by low temperature helium adsorption. J. Phys. Chem. **100**, 10331–10336 (1996)

Sing, K.S.W., Everett, D.H., Haul, R.A.W., Moscou, L., Pierotti, R.A., Rouquérol, J., Siemieniewska, T.: Reporting physisorption data for gas/solid systems with special reference to the determination of surface area and porosity. Pure Appl. Chem. **57**, 603–619 (1985)

Sircar, S.: Gibbsian surface excess for gas adsorption—revisited. Ind. Eng. Chem. Res. **38**, 3670–3682 (1999)

Skouri, M., Marignan, J., May, R.: X-Ray and neutron-scattering study of the lamellar and L_3 phases of the system aerosol-OT-water effect of NaCI and decane. Colloid Polym. Sci. **269**, 929–937 (1991)

Stefanopoulos, K.L., Romanos, G.E., Vangeli, O.C., Mergia, K., Kanellopoulos, N.K., Koutsioubas, A., Lairez, D.: Investigation of confined ionic liquid in nanostructured materials by a combination of SANS, contrast-matching SANS, and nitrogen adsorption. Langmuir **27**, 7980–7985 (2011)

Steriotis, Th.A., Stefanopoulos, K.L., Keiderling, U., De Stefanis, A., Tomlinson, A.A.G.: Characterisation of pillared clays by contrast-matching small-angle neutron scattering. Chem. Commun. **20**, 2396–2397 (2002a)

Steriotis, T.A., Stefanopoulos, K.L., Mitropoulos, A.C., Kanellopoulos, N.K., Hoser, A., Hofmann, M.: Structural studies of supercritical carbon dioxide in confined space. Appl. Phys. A, Mater. Sci. Process. **74**, S1333–S1335 (2002b)

Steriotis, Th.A., Stefanopoulos, K.L., Kanellopoulos, N.K., Mitropoulos, A.C., Hoser, A.: The structure of adsorbed CO_2 in carbon nanopores: a neutron diffraction study. Colloids Surf. A, Physicochem. Eng. Asp. **241**, 239–244 (2004)

Steriotis, Th.A., Stefanopoulos, K.L., Katsaros, F.K., Gläser, R., Hannon, A.C., Ramsay, J.D.F.: In situ neutron diffraction study of adsorbed carbon dioxide in a nanoporous material: monitoring the adsorption mechanism and the structural characteristics of the confined phase. Phys. Rev. B **78**, 115424 (2008)

Zhang, B., Wang, T., Liu, S., Zhang, S., Qiu, J., Chen, Z., Cheng, H.: Structure and morphology of microporous carbon membrane materials derived from poly(phthalazinone ether sulfone ketone). Microporous Mesoporous Mater. **96**, 79–83 (2006)

Zickler, G.A., Jähnert, S., Wagermaier, W., Funari, S.S., Findenegg, G.H., Paris, O.: Physisorbed films in periodic mesoporous silica studied by in situ synchrotron small-angle diffraction. Phys. Rev. B **73**, 184109 (2006)